Deep-Sea Research II 56 (2009) 2936–2947

Contents lists available at ScienceDirect

Deep-Sea Research II

journal homepage: www.elsevier.com/locate/dsr2

Influences of initial plankton biomass and mixed-layer depths on the outcome of iron-fertilization experiments

M. Fujii [a,*], F. Chai [b]

[a] Sustainability Governance Project, Center for Sustainability Science, Hokkaido University, N9W8, Kita-ku, Sapporo, Hokkaido 060-0809, Japan
[b] School of Marine Sciences, 5706 Aubert Hall, University of Maine, Orono, ME 04469-5706, USA

ARTICLE INFO

Topical issue on "SEEDS II: The Second Subarctic Pacific Iron Experiment for Ecosystem Dynamics Study." The issue is compiled and guest-edited by the North Pacific Marine Science Organization (PICES) and International SOLAS.
Available online 17 July 2009

Keywords:
Iron-enrichment experiments
Modeling
Initial plankton biomass
Mixed-layer depth
Diatom bloom
Grazing

ABSTRACT

Several *in situ* iron-enrichment experiments have been conducted, where the response of the phytoplankton community differed. We use a marine ecosystem model to investigate the effect of iron on phytoplankton in response to different initial plankton conditions and mixed-layer depths (MLDs). Sensitivity analysis of the model results to the MLDs reveals that the modeled response to the same iron enhancement treatment differed dramatically according to the different MLDs. The magnitude of the iron-induced biogeochemical responses in the surface water, such as maximum chlorophyll, is inversely correlated with MLD, as observed. The significant decrease in maximum surface chlorophyll with MLD results from the difference in diatom concentration in the mixed layer, which is determined by vertical mixing. The modeled column-integrated chlorophyll, on the other hand, is the highest with intermediate MLD cases, suggesting difference in iron-induced biogeochemical responses between volume and area considerations. The iron-induced diatom bloom is severely restricted below the compensation depth due to both light limitation and grazing pressure, irrespective of the MLD. Sensitivity of the model to initial mesozooplankton (as grazers on diatoms) biomass shows that column-integrated biomass, net community production and export production are strongly controlled by the initial mesozooplankton biomass. Higher initial mesozooplankton biomass yields high grazing pressure on diatoms, which results in less accumulation of diatom biomass and may account for notably lower surface chlorophyll during SEEDS (Subarctic Pacific Iron Experiment for Ecosystem Dynamics Study) II than during SEEDS. The initial diatom biomass is also important to the outcome of iron enrichment but is not as crucial as the MLD and the initial mesozooplankton biomass. This modeling study suggests that not only MLD but also the initial biomass of diatoms and its principle grazers are crucial factors in the response of the phytoplankton community to iron enrichments, and should be considered in designing future iron-enrichment experiments.

1. Introduction

In high-nutrient, low-chlorophyll (HNLC) regions, the availability of iron to phytoplankton plays an important role in determining phytoplankton growth (e.g., Martin and Fitzwater, 1988; Banse, 1990; Martin, 1990). To confirm this iron-limitation hypothesis, several *in situ* iron-enrichment experiments have been conducted in the HNLC regions (e.g., Coale et al., 1996, 2004; Boyd et al., 2000, 2004, 2007; Gervais et al., 2002; Tsuda et al., 2003). However, the observed responses of the phytoplankton communities are dramatically different among these iron experiments in the HNLC regions (e.g., de Baar et al., 2005; Fujii et al., 2005). For example, the iron-induced maximum surface chlorophyll and decrease of pCO_2 at the surface ($pCO_{2\,sea}$) were as large as 19 ($mg\,m^{-3}$) and 94 (μatm) at SEEDS (the Subarctic Pacific Iron Experiment for Ecosystem Dynamics Study) in the subarctic western North Pacific (Tsuda et al., 2003), but as small as 2 ($mg\,m^{-3}$) and 20 through 30 (μatm) at SOIREE (The first Southern Ocean Iron Release Experiment; Boyd et al., 2000) and EisenEx (The Carbondioxide Uptake Southern Ocean (CARUSO)/Eisen(= Iron) Experiment; Gervais et al., 2002; Bakker et al., 2005) in the Southern Ocean.

Through comparison of eight iron experiments, de Baar et al. (2005) showed that the iron-induced maximum chlorophyll, the maximum dissolved inorganic carbon (DIC) removal and the overall DIC/Fe efficiency all scale inversely with the mixed-layer depth (MLD) defining the light environment, and that lateral patch dilution, sea-surface irradiance, temperature and grazing

* Corresponding author. Now at: Graduate School of Environmental Science, Hokkaido University, N10W5, Kita-ku, Sapporo, Hokkaido 060-0810, Japan.
Tel.: +81 11 706 2359; fax: +81 11 706 4867.
E-mail address: mfujii@ees.hokudai.ac.jp (M. Fujii).

0967-0645/$ - see front matter © 2009 Elsevier Ltd. All rights reserved.
doi:10.1016/j.dsr2.2009.07.007

play additional roles. Applying a marine ecosystem model to SEEDS, Fujii et al. (2005) used sensitivity analysis to show that water temperature significantly controls both the timing and magnitude of iron-induced diatom bloom, and that the e-ratio (a ratio of export production (EP) to net community production (NCP)) is inversely correlated with temperature. Their model sensitivity studies on the duration of iron enrichment also revealed that multiple iron infusions for longer than a week would not be effective in SEEDS because of the stronger silicate limitations during the later phase of the diatom bloom. In other words, the initial dissolved silicate does affect the duration of bloom, although formal sensitivity analysis of initial dissolved silicate was not conducted. These previous observational and modeling studies suggest that the physical and chemical environmental conditions, other than iron, are also predominant factors in controlling biogeochemical responses to iron enrichments.

On the other hand, recent observational data have shown that the increases in phytoplankton biomass inside the iron patch were dramatically different between SEEDS and SEEDS II, which were conducted in the same location and at the same season of the year (Tsuda et al., 2007), when physical and chemical environmental conditions were very similar. These results imply that factors other than just physical and chemical environmental conditions could also significantly determine the response of the phytoplankton community to iron addition. Several previous studies (Landry et al., 2000a, b; Rollwagen Bollens and Landry, 2000; Jansen et al., 2006; Schultes et al., 2006) suggested that grazing processes and/or major nutrient limitations regulate iron-induced phytoplankton biomass accumulation. Grazing pressure is also related to the initial zooplankton biomass when iron is being introduced to the experimental site. Since the initial physical, chemical and plankton conditions may vary widely among different iron-enrichment experiments, it is difficult to isolate, solely by observation, the key factors that regulate the iron-induced phytoplankton bloom. This necessitates more rigorous verification by application of a generic plankton ecosystem simulation model to the iron experiments (de Baar et al., 2005).

Taking into consideration the suite of environmental variables each of which, more or less, controls the response to *in situ* iron fertilization, sensitivity to water temperature and duration of SEEDS have previously been assessed (Fujii et al., 2005), with additional implications for sensitivity to initial dissolved silicate. Sensitivity to variations of incident irradiance on the one hand is so strong that it is deemed low priority for special study. On the other hand lateral patch dilution has been so poorly defined in field observations thus far that it first requires a sophisticated dilution/mixing description, before sensitivity analysis in a plankton ecosystem simulation model can be feasible. Presumably the lateral patch dilution is an important physical factor that controls biological responses to iron-fertilization experiments (Assmy et al., 2007) and the effect is examined by using a 3D ecosystem model that can reproduce explicitly the lateral patch dilution (e.g., Chai et al., in preparation).

Here, we use a marine ecosystem model to examine the response of the phytoplankton community to selected different physical environmental conditions and different initial plankton conditions, focusing on the sensitivity of model results to MLD and the initial biomass of diatoms and mesozooplankton, the latter being major grazers of diatoms. In the following section we describe the ecosystem model to be used and the experimental design with changes in MLD and initial plankton biomass. The results based on variations of SEEDS and their implications also for other fertilization experiments are discussed in Section 3 and a summary is presented in Section 4.

2. Model description and experimental design

We used a 16-compartment marine ecosystem model (e.g., Fujii et al., 2002, 2005; Yamanaka et al., 2004; Fig. 1). In this model, phytoplankton and zooplankton are categorized by their functional groups in view of the food web (Landry et al., 2000a, b; Rollwagen Bollens and Landry, 2000; Hall and Safi, 2001; Hannon et al., 2001; Tsuda et al., 2003; Suzuki et al., 2005; Takeda and Tsuda, 2005; Saito et al., 2005, 2006; Jansen et al., 2006; Schultes et al., 2006).

Phytoplankton are categorized into two groups: large diatoms (PL), including large chain-forming centric diatoms *Chaetoceros debilis*, and smaller phytoplankton (PS), including autotrophic nanoflagellates and coccolithophorids. Phytoplankton components utilize nitrate (NO_3) and ammonia (NH_4) in the process of photosynthesis and produce soft tissue in the form of particulate organic nitrogen (PON). Along with photosynthesis, diatoms utilize silicate ($Si(OH)_4$) to produce frustules in the form of biogenic silica.

Zooplankton are categorized into three groups: diatom-grazing micro- or mesozooplankton (ZL), including copepoda and ciliates, predatory macrozooplankton (ZP), including carnivorous *Chaetogratha*, and other non-diatom-grazing microzooplankton (ZS), including foraminifera. Coccolithophorids and foraminifera produce hard shells of calcium carbonate ($CaCO_3$). Detailed zooplankton dynamics, such as the ontogenetic vertical migration and the reproductive cycle, are not considered in the current modeling study. These processes may not influence model results for a short experimental period (60 days or less) and during the summer months in a significant way. Recent observational outcome reveals that the vertical migration of zooplankton contributes to an extra export term not captured in the sediment traps by bypassing the sediment traps (Saito et al., 2009). This mechanism is beyond the scope of the current model but is worth being taken into account.

Total alkalinity (TAlk) is calculated by the balances of $CaCO_3$, NO_3 and NH_4. The dissolved inorganic carbon is calculated by balances of TAlk, NO_3 and NH_4 (with a carbon to nitrogen ratio of 6.625; Redfield et al., 1963). Therefore, the partial pressure of CO_2 at the sea surface ($pCO_{2\,sea}$) is calculated and the air–sea CO_2 flux can be estimated by this model.

The ecosystem model is coupled with a one-dimensional mixed-layer model. The mixed-layer model has 20 layers vertically between the surface and a depth of 100 m, with vertical resolution of 5 m. The physical–biogeochemical model is applied to the location and period of SEEDS (from 18 to 31 July 2001 at 48.5°N, 165°E), an iron-enrichment experiment in the subarctic western North Pacific (Tsuda et al., 2003; Takeda and Tsuda, 2005). Although the model structure, forcing functions and parameter values are similar to those described by Fujii et al. (2005), a few modifications to the model experimental design from Fujii et al. (2005) are carried out to directly compare the model results with observations in the eight iron-enrichment experiments described in de Baar et al. (2005). The daily averaged photosynthetically active radiation (PAR) at the sea surface in a standard experiment, which was given to vary with season in Fujii et al. (2005), is fixed to 75.1 ($W\,m^{-2}$; de Baar et al., 2005) during the simulation period of 60 days. The MLD at SEEDS I was fixed to 25 and 12.5 m in Fujii et al. (2005) and de Baar et al. (2005), respectively. In this study, we fixed the MLD to 12.5 m because this value is considered as a better representative of the observed MLD at SEEDS. The water temperature is given so that the temperature is uniform in the MLD and the heat content is conserved in the water column.

In this model, the diatom growth rate is calculated as the product of the maximum growth rate, water temperature

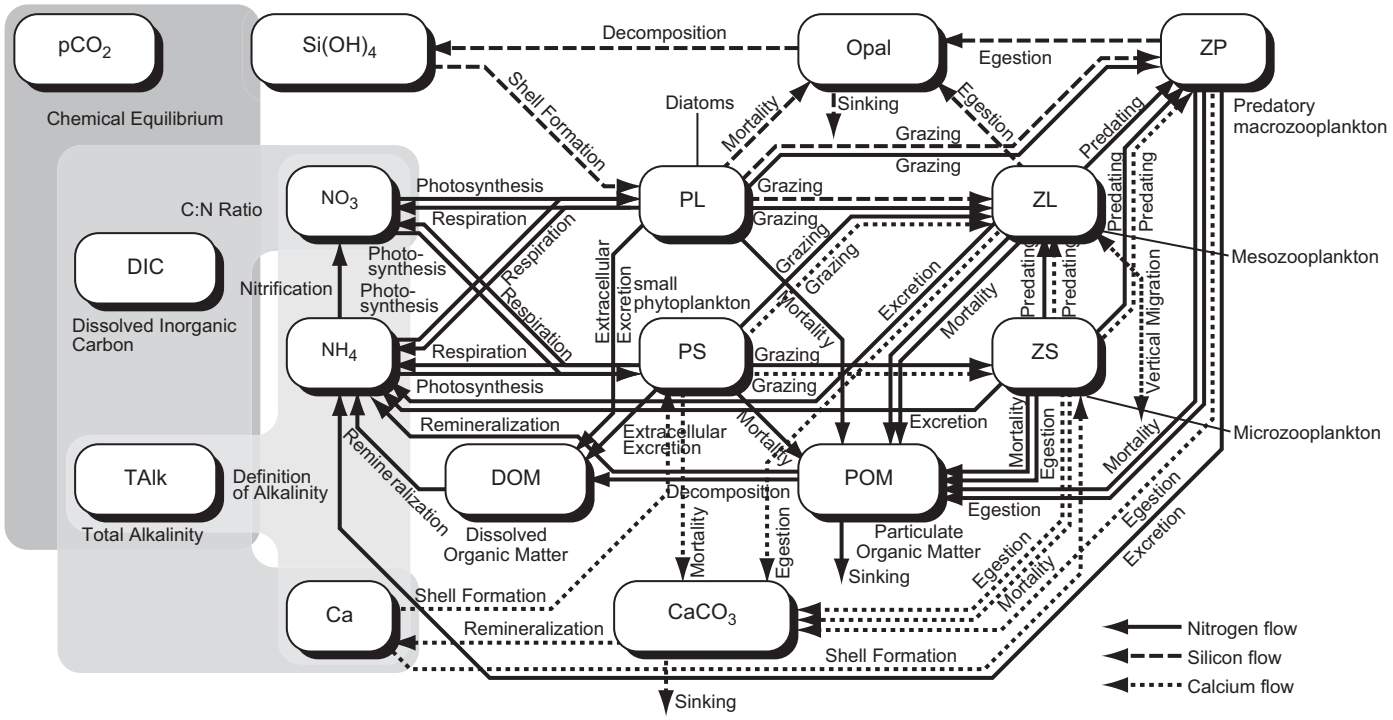

Fig. 1. Schematic view of the sixteen-compartment marine ecosystem model after Fujii et al. (2002, 2005) and Yamanaka et al. (2004). Here PS (mmol N m^{-3}) is non-diatom smaller phytoplankton biomass, PL (mmol N m^{-3}) is diatom biomass, ZS (mmol N m^{-3}) is non-diatom-grazing microzooplankton biomass, ZL (mmol N m^{-3}) is diatom-grazing micro- or mesozooplankton biomass, ZP (mmol N m^{-3}) is predatory macrozooplankton biomass, NO_3 (mmol N m^{-3}) is dissolved nitrate, $Si(OH)_4$ (mmol Si m^{-3}) is dissolved silicate, DIC (mmol C m^{-3}) is total CO_2 or the complete pool of dissolved inorganic carbon in seawater and $pCO_{2\,sea}$ (μatm) is the partial pressure of CO_2 in seawater. The additional pools are active and dynamic part of the model simulations but not discussed in the text: NH_4 (mmol N m^{-3}) is dissolved ammonia, POM (mmol N m^{-3}) is particulate organic matter, DOM (mmol N m^{-3}) is dissolved organic matter, Opal (mmol Si m^{-3}) is opal or biogenic silica frustules of diatoms, Ca (mmol Ca m^{-3}) is total dissolved calcium, $CaCO_3$ (mmol C m^{-3}) is biogenic calcium carbonate or shells and TAlk (mmol m^{-3}) is total alkalinity.

dependence (Q_{10} effect), light regulation, nutrient (NO_3, NH_4 and $Si(OH)_4$) controls and diatom concentration, as follows:

$$\text{diatom total growth rate} = \underbrace{V_{\max L}}_{\text{Term 1}}\underbrace{\exp(k_L T)}_{\text{Term 2}} \times \underbrace{\min\left\{\frac{[NO_3]}{[NO_3]+K_{NO_{3L}}}\exp(-\Psi_L[NH_4])+\frac{[NH_4]}{[NH_4]+K_{NH_{4L}}},\ \frac{[Si(OH)_4]}{[Si(OH)_4]+K_{SiL}}\right\}}_{\text{Term 3}}$$
$$\times \underbrace{\left\{1-\exp\left(\frac{-\alpha\times PAR}{V_{\max L}}\right)\right\}}_{\text{Term 4}} \times \underbrace{[\text{diatom biomass}]}_{\text{Term 5}}, \quad (1)$$

where T is the water temperature (°C), $V_{\max L}$ the maximum growth rate (day^{-1}) and α the initial slope of the photosynthesis–irradiance (P vs. I) curve ($W^{-1}\,m^2\,day^{-1}$). See Table 2 in Fujii et al. (2005) for other abbreviations. Following Fujii et al. (2005), the nutrient phosphate is not taken into account as is usual in most plankton ecosystem models, while trace nutrient iron is implicit in $V_{\max L}$ and α as explained below.

In this model, diatoms are set to be grazed on mainly by mesozooplankton and a small portion (~10%) by macrozooplankton. The grazing on diatoms by mesozooplankton, or the total grazing rate, is expressed as the product of the maximum grazing rate, water temperature dependence (Q_{10} effect), and biomass of both diatoms and mesozooplankton, as follows:

$$\begin{aligned}&\text{total grazing rate on diatoms by mesozooplankton}\\&= G_{R\max PL}\exp(k_G T)\\&\quad\times\max\{0, 1-\exp(-\lambda[\text{diatom biomass}])\}\\&\quad\times[\text{mesozooplankton biomass}].\end{aligned} \quad (2)$$

In order to simulate the effects of iron enrichment in this model, the values of $V_{\max L}$ (day^{-1}) and α ($W^{-1}\,m^2\,day^{-1}$) for diatoms are set to increase linearly from Day 0 (the date on which iron was infused into the surface water) to Day 3, to be kept at the maxima (three times higher than the initial values) until Day 10, and to decrease linearly to the initial values at Day 20 (Fig. 2), which is the same manner used in Fujii et al. (2005). We also increased the values of the chlorophyll–carbon ratio by weight for diatoms during the iron-enrichment period in the same manner (Fig. 2), and found the model reproduces better the observed chlorophyll than that with the ratio fixed to 1:50 (Fujii et al., 2005).

Using a higher maximum specific growth rate for diatoms is equivalent to removing or greatly reducing all physiological limitations due to trace nutrients such as iron. By keeping all other model parameters the same, including the grazing formulation, the effect of removing a physiological constraint on photosynthetic performance or growth can be distinguished from the effects of physical processes and grazing. Similar procedures have been used in previous modeling studies to investigate the

effect and impact of iron fertilization on phytoplankton growth dynamics (Denman and Peña, 1999; Chai et al., 2002, 2007; Fujii et al., 2005; Yoshie et al., 2005). Notice that this merely simulates the role of iron in SEEDS, whereas a dedicated sensitivity analysis for realistic iron concentration is the subject of ongoing studies (e.g., Sato et al., in preparation).

To investigate the effects on the phytoplankton community in response to different MLD and initial plankton conditions, we conducted several sets of model sensitivity studies (Table 1) in reference to realistic observed ranges (e.g., de Baar et al., 2005; Tsuda et al., 2007). The first set of experiments investigates the role of MLD, the maximum of which is fixed at 7.5 (Case 1-1), 12.5 (Case 1-2; standard case), 17.5 (Case 1-3), 22.5 (Case 1-4), 27.5 (Case 1-5), 47.5 (Case 1-6) and 72.5 m (Case 1-7) (Experiment 1). The second set of experiments studied the role of initial diatom biomass on Day 0, which was set at 0.001 (Case 2-1), 0.01 (Case 2-2), 0.1 (Case 2-3), 1 (Case 2-4; standard case), 10 (Case 2-5), 100 (Case 2-6), and 1000 (Case 2-7) times the standard initial condition used in Fujii et al. (2005) (Experiment 2). The initial mesozooplankton biomass on Day 0 was set at 0.01 (Case 3-1), 0.1 (Case 3-2), 1 (Case 3-3; standard case), 5 (Case 3-4), 10 (Case 3-5), 20 (Case 3-6) and 30 (Case 3-7) times the standard value as used in Fujii et al. (2005) (Experiment 3). Additional experiments 4–6 (see Table 1) were done with similar variations in the initial biomass of non-diatom small phytoplankton PS (Experiment 4), microzooplankton ZS (Experiment 5) and predatory macrozooplankton ZP (Experiment 6), respectively.

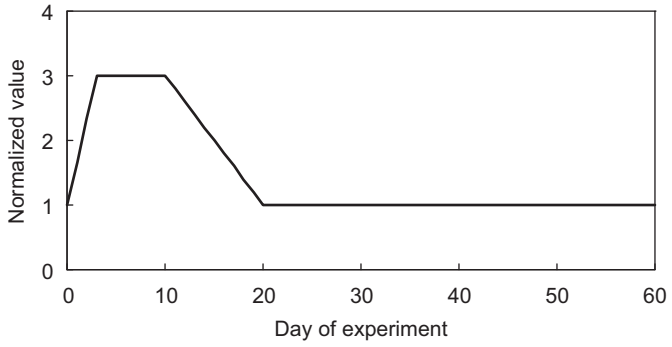

Fig. 2. Temporal changes of the maximum growth rate V_{maxL} (day^{-1}), the initial slope α ($W^{-1}\,m^2\,day^{-1}$) of photosynthesis–irradiance (P vs. I) curve and the chlorophyll–carbon ratio by weight for diatoms in the model from Day 0 to 60. All three variables are set to follow identical relative changes as follows: an increase linearly from Day 0 (the date on which iron was infused to the surface water) to Day 3, to be kept at the maxima (by 3 times as high as the initial values) until Day 10, to decrease linearly to the initial values on Day 20 and then remain constant over the Days 20–60 period.

3. Results and discussion

We evaluated the model performance using the SEEDS results, which served as a reference state. In comparison with SEEDS observations, the model results in the standard case (Cases 1-2, 2-4 and 3-3; they are identical) reproduce the observations reasonably well after iron infusion, i.e., a rapid increase in surface chlorophyll and decreases in surface nutrients and $pCO_{2\,sea}$ (black solid lines in Fig. 3). These changes are caused by a diatom bloom stimulated by iron infusion. A detailed analysis of the standard case was presented in Fujii et al. (2005) and Yoshie et al. (2005).

3.1. Biogeochemical responses to mixed-layer depth

In Experiment 1, the water temperature is uniform in the mixed layer and decreases with an increase of MLD, from 9.3 °C in Case 1-1 (MLD = 7.5 m) to 4.3 °C in Case 1-7 (MLD = 72.5 m; Fig. 4(A)). The water temperature in the mixed layer shows an inverse relationship with the MLD ($R^2 = 0.97$; Fig. 4(B)). Fig. 4(C) shows the mixed-layer-mean PAR on the date when the iron-induced surface chlorophyll concentration is maximum, that is, on Days 11, 12, 13, 13, 14, 16 and 18 in Cases 1-1, 1-2, 1-3, 1-4, 1-5, 1-6 and 1-7, respectively. The mixed-layer-mean PAR also decreases with an increase of MLD, from 18.0 ($W\,m^{-2}$) in Case 1-1 to 9.3 ($W\,m^{-2}$) in Case 1-7, and is inversely correlated with the MLD ($R^2 = 0.79$; Fig. 4(C)).

The modeled iron-induced biogeochemical responses, namely the rapid increase in surface chlorophyll and decreases in surface nutrients and $pCO_{2\,sea}$, occur earlier and are larger with shallower MLD cases (Fig. 3(A)). The maximum surface chlorophyll, and the maximum differences between inside and outside the iron patch for surface silicate ($\Delta Si(OH)_4$), surface DIC (ΔDIC), $pCO_{2\,sea}$ ($\Delta pCO_{2\,sea}$), column-integrated chlorophyll, NCP above 100 m depth (ΔNCP) and EP at 100 m depth (ΔEP), are plotted in Fig. 5-1. The model results show a striking and significant inverse relationship ($R^2 > 0.94$) between each variable and MLD, consistent with observations from the eight iron-enrichment experiments (de Baar et al., 2005). This suggests that the inverse relationship between MLD and iron-induced biogeochemical responses is a robust feature, which has been documented both in this model of SEEDS and in other observations (de Baar et al., 2005).

Although the surface values have their peaks in Case 1-1 (MLD = 7.5 m), some of the maximal column-integrated values appear with intermediate MLD cases (Fig. 5-1). For example, unlike the maximum surface chlorophyll, the column-integrated chlorophyll is the highest in Case 1-3 (MLD = 17.5 m; Fig. 5-1(E)).

Table 1
Model experimental design.

Experiment number	Changing parameter (unit)	Symbol	Fluctuation range						
1	Mixed-layer depth (m)	MLD	7.5 (1–1)	**12.5 (1–2)**	17.5 (1–3)	22.5 (1–4)	27.5 (1–5)	47.5 (1–6)	72.5 (1–7)
2	Initial diatom biomass (mmol C m^{-3})	PL	0.001 × (2–1)	0.01 × (2–2)	0.1 × (2–3)	**1 × (2–4)**	10 × (2–5)	100 × (2–6)	1000 × (2–7)
3	Initial mesozooplankton biomass (mmol C m^{-3})	ZL	0.01 × (3–1)	0.1 × (3–2)	**1 × (3–3)**	5 × (3–4)	10 × (3–5)	20 × (3–6)	30 × (3–7)
4	Initial non-diatom small phytoplankton biomass (mmol C m^{-3})	PS	0.001 × (4–1)	0.01 × (4–2)	0.1 × (4–3)	**1 × (4–4)**	10 × (4–5)	100 × (4–6)	1000 × (4–7)
5	Initial microzooplankton biomass (mmol C m^{-3})	ZS	0.01 × (5–1)	0.1 × (5–2)	**1 × (5–3)**	5 × (5–4)	10 × (5–5)	20 × (5–6)	30 × (5–7)
6	Initial predatory macrozooplankton biomass (mmol C m^{-3})	ZP	0.01 × (6–1)	0.1 × (6–2)	**1 × (6–3)**	5 × (6–4)	10 × (6–5)	20 × (6–6)	30 × (6–7)

Case numbers are shown in parentheses below the given fluctuation range. Cases 1-2, 2-4, 3-3, 4-4, 5-3 and 6-3 in bold print are the standard experiments (they are identical). Variations of MLD (Experiment 1), initial diatom biomass PL (Experiment 2) and initial mesozooplankton biomass ZL (Experiment 3) have been shown to be far more significant than variations of initial non-diatom small phytoplankton biomass PS (Experiment 4), initial microzooplantkon biomass ZS (Experiment 5) and initial predatory macrozooplankton biomass ZP (Experiment 6).

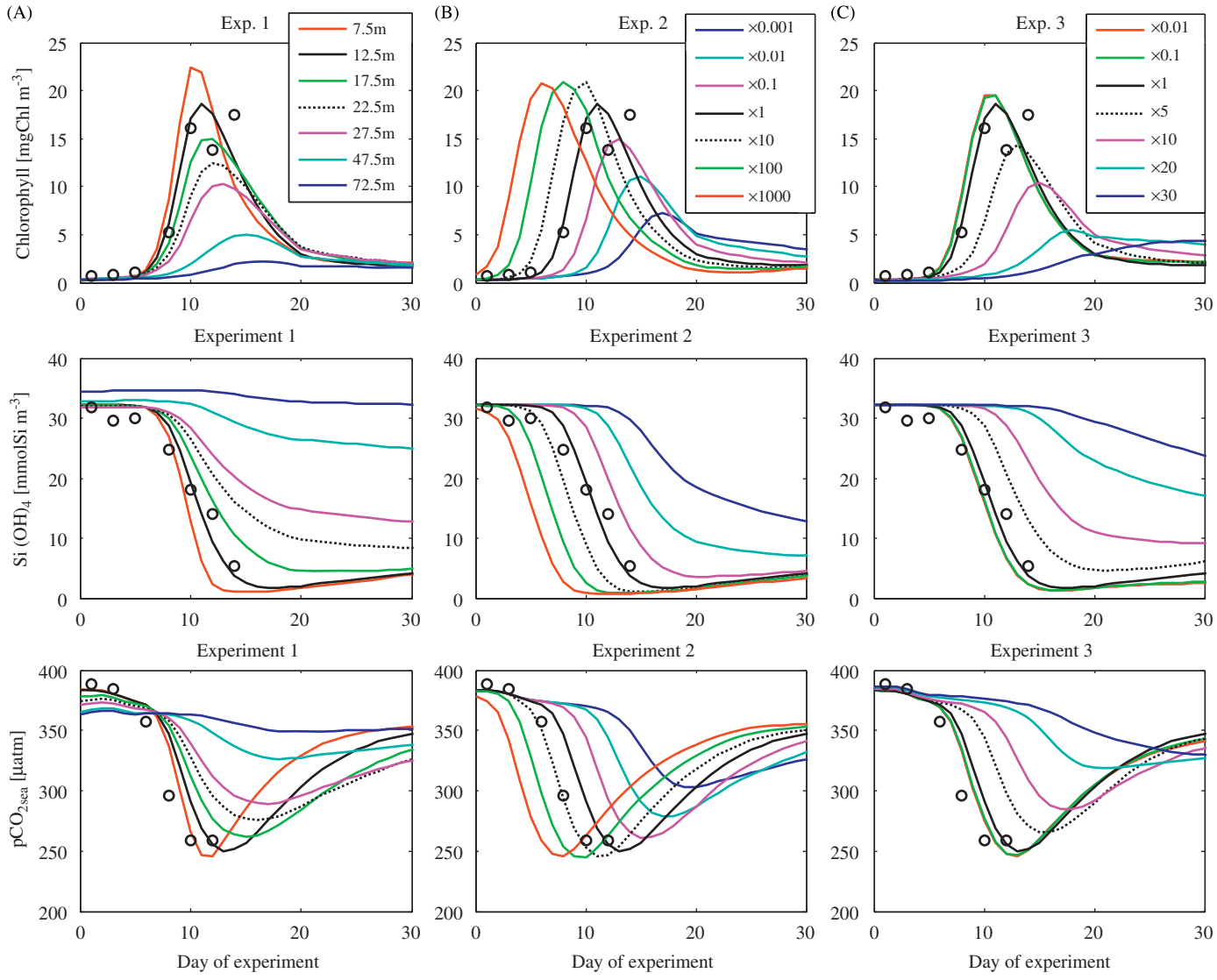

Fig. 3. Time series of modeled surface chlorophyll (mg Chl m^{-3}), $Si(OH)_4$ (mmol Si m^{-3}), and $pCO_{2\,sea}$ (µatm) in (A) Experiment 1 varying mixed-layer depth MLD, (B) Experiment 2 varying initial diatom biomass PL and (C) Experiment 3 varying initial mesozooplankton biomass ZL. Black solid lines show model results of the standard experiment (Cases 1-2, 2-4 and 3-3). Open circles denote field observation data from SEEDS (Tsuda et al., 2003).

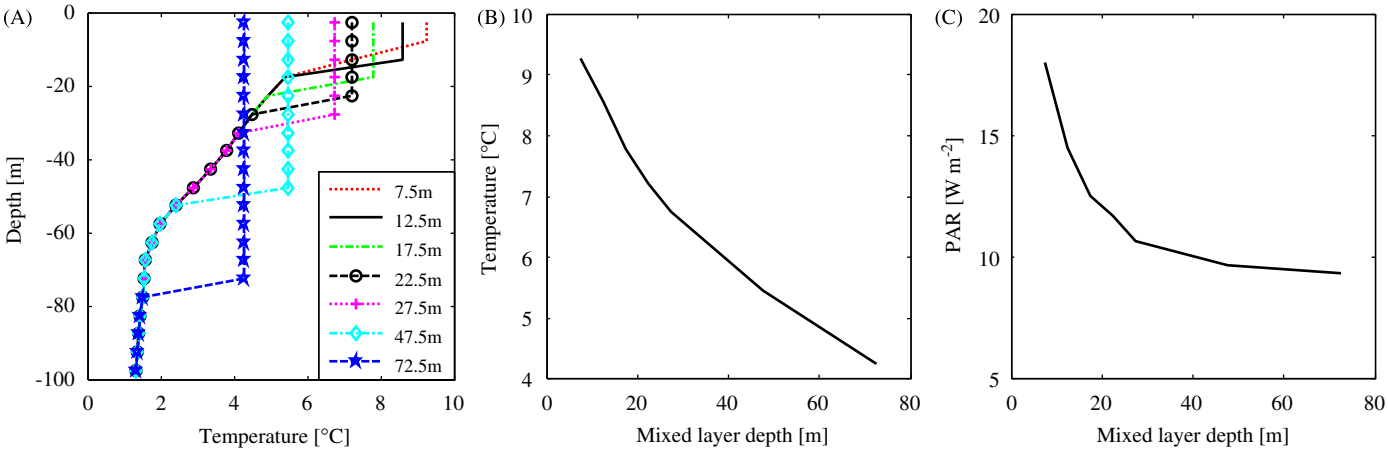

Fig. 4. Modeled (A) vertical profile of water temperature (°C), (B) water temperature in the mixed layer (°C) vs. the mixed-layer depth MLD (m) and (C) mean PAR in the mixed layer (W m^{-2}) vs. MLD (m) all in Experiment 1 varying MLD.

The modeled ΔEP has its peak of 1908.8 (mg C m^{-2} day^{-1}) in Case 1-2 (MLD = 12.5 m; Fig. 5-1(G)). This is due to greater decomposition of the particulate organic carbon in the MLD in Case 1-1 than in Case 1-2, resulting from higher water temperature in Case 1-1 (Fig. 4(A)). Previous studies show that the e-ratio is inversely correlated with water temperature (e.g., Laws et al., 2000; Fujii et al., 2005). On the other hand, the surface water temperature was much more diverse among the eight iron-enrichment experiments (−0.5 through 25.2 °C; de Baar et al., 2005) than in this study (4.3–9.3 °C; Fig. 4(B)) and there is no clear correlation between the observed MLD and surface water temperature ($R^2 = 0.32$). Therefore, ΔEP in the eight iron-enrichment experiments is unlikely to have an inverse relationship with MLD. EP is an essential variable for assessing the efficiency of the oceanic carbon uptake by iron-enrichment experiments, although the export of carbon into deeper waters is difficult to estimate and, to date, has been proven quite modest in only two iron experiments (de Baar et al., 2005).

We examined the predominant factors that cause the notable inverse relationship between the maximum surface chlorophyll and MLD, by comparing the modeled magnitude of terms in Eq. (1). Fig. 6 shows the vertical profiles of Terms 1–5 in Eq. (1), the diatom-specific growth rate (equivalent to the product of Terms 1–4), and the diatom total growth rate (equivalent to the product of the diatom-specific growth rate and Term 5), on the date when the maximum surface chlorophyll appears (on Days 11, 12, 13, 13, 14, 16 and 18 in Cases 1-1, 1-2, 1-3, 1-4, 1-5, 1-6, and 1-7, respectively). The maximum diatom growth rate (Term 1; Fig. 6(A)) is higher in Case 1-1 (MLD = 7.5 m) than in Case 1-7 (MLD = 72.5 m) by a factor of 1.9, because the maximum surface chlorophyll appears earlier in shallower MLD cases (Figs. 2 and 3(A)). The temperature dependence term (Term 2; Fig. 6(B)) is larger in Case 1-1 than in Case 1-7 by a factor of 1.2 due to higher water temperatures in shallower MLD cases (Fig. 4(A)). The nutrient limitation (Term 3; Fig. 6(C)), by contrast, is weaker in Case 1-7 than in Case 1-1 by a factor of 1.1 due to higher nutrient

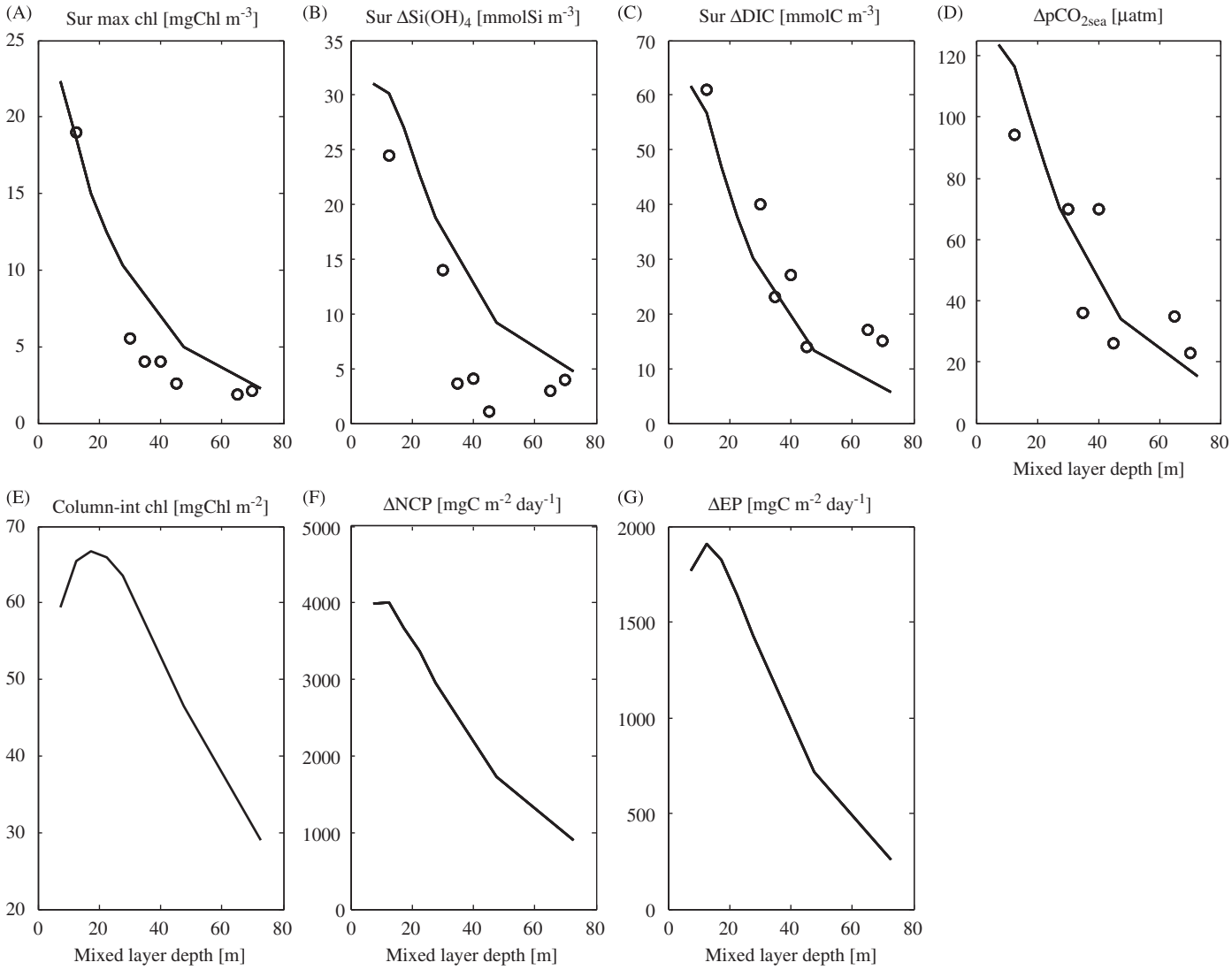

Fig. 5. (1) (A) Surface maximum chlorophyll (mg Chl m^{-3}), (B) Δ $Si(OH)_4$ (mmol Si m^{-3}), (C) Δ DIC (mmol C m^{-3}), (D) Δ $pCO_{2\,sea}$ (μatm), (E) column-integrated chlorophyll (mg Chl m^{-2}), (F) Δ NCP (mg C m^{-2} day^{-1}) and (G) ΔEP (mg C m^{-2} day^{-1}) all vs. the mixed-layer depth MLD (m) in Experiment 1 varying MLD. Open circles denote field observation data from eight iron-enrichment experiments (de Baar et al., 2005). (2) Same as (1) but for Experiment 2 varying the initial diatom biomass PL (filled diamonds), Experiment 3 varying the initial mesozooplankton biomass ZL (filled dots) and Experiment 4 varying the initial non-diatom small phytoplankton biomass PS (dotted line).

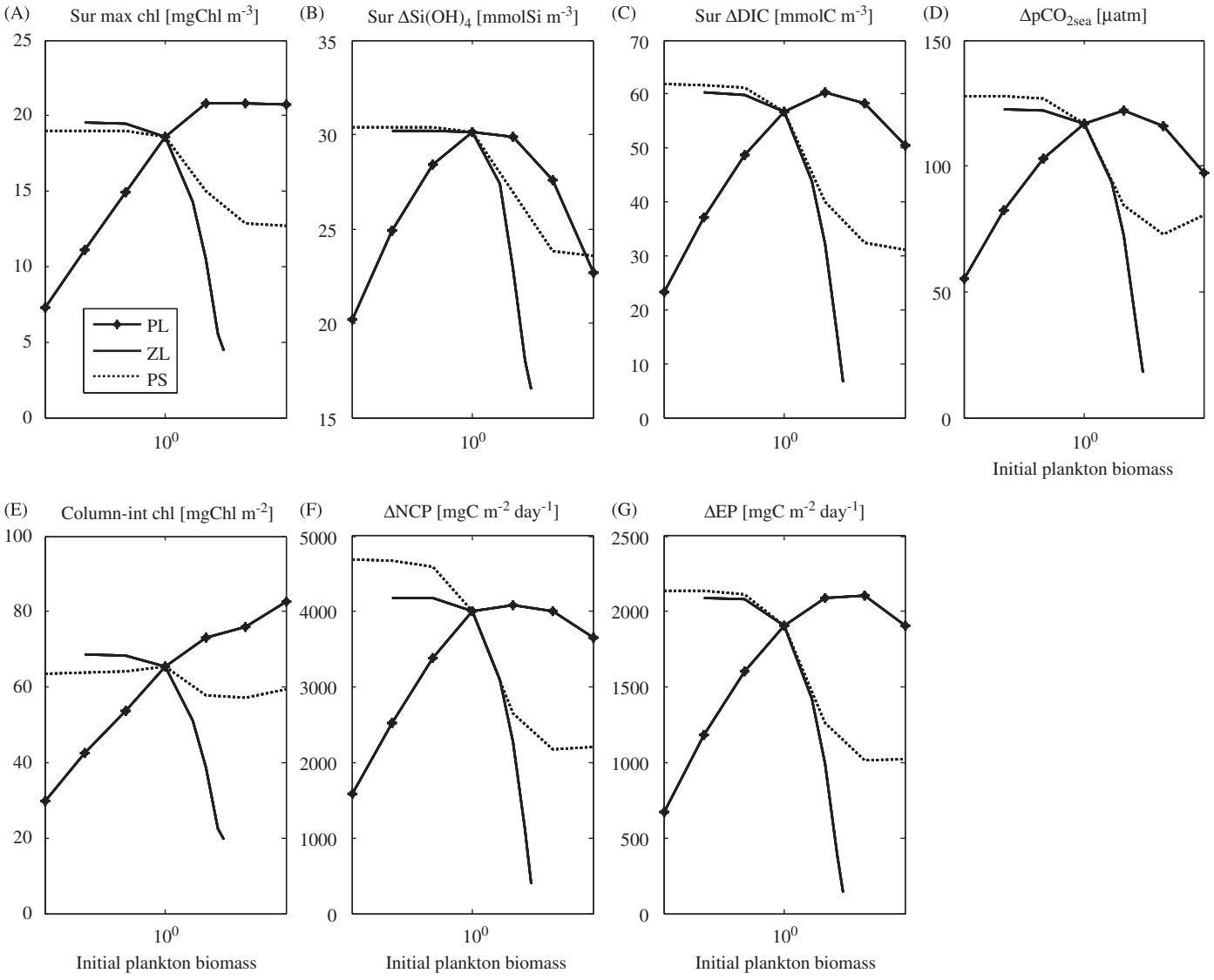

Fig. 5. (*Continued*)

concentrations in deeper MLD cases (Fig. 3(A)). The modeled compensation depth, defined as the depth at which PAR is equal to 1% of the surface PAR, was calculated and compared to the MLD (Table 2). The compensation depth is almost the same as the MLD in Case 1-5, and is deeper and shallower than the MLD in Cases 1-1 through 1-4 and Cases 1-6 through 1-7, respectively. This suggests that phytoplankton in deeper MLD cases (Cases 1-6 and 1-7) are exposed to light limitation when they are pushed down to deeper layers by vertical mixing. Interestingly, on the other hand, the light limitation (Term 4; Fig. 6(D)) at each depth is stronger in shallower MLD cases, because self-shading by the more abundant phytoplankton diminishes the available light below. Light limitation in the surface water is slightly stronger in Case 1-1 than in Case 1-7 but only by a factor of 1.1. As a result, the diatom-specific growth rate (Fig. 6(E)) is higher by a factor of 1.7 at the surface, but it is lower in subsurface layers in Case 1-1 than in Case 1-7.

The most significant difference among the MLD cases is the diatom biomass (Term 5; Fig. 6(F)). The diatom biomass is uniform within the mixed layer because of vertical mixing, and it is larger in Case 1-1 than in Case 1-7 by a factor of 7.1. Also the surface maximum chlorophyll differs between the cases by a factor of 10.0 (Fig. 5-1(A)). Consequently, the diatom total growth rate at the surface (Fig. 6(G)) is much higher in Case 1-1 than in Case 1-7 by a factor of 12.3, primarily due to the larger diatom biomass. The diatom total growth rate decreases exponentially with depth in any case, but more rapidly in shallower MLD cases because of rapid decreases in both diatom-specific growth rate and diatom biomass with depth. Therefore, depth integration of the diatom total growth rate, namely the NCP, partly compensates the advance effects of a deep MLD, decreasing the differences in responses among the cases to a factor of 4.4 (Fig. 5-1(F); de Baar et al., 2005).

The modeled diatom total growth rate was compared with the corresponding total grazing rate on diatoms by zooplankton (ZL and ZP) on the date when the maximum surface chlorophyll appears (Figs. 6(H) and (I)). The total grazing rate on diatoms by zooplankton has a similar vertical profile to the diatom biomass in any cases, because the grazing rate depends on the diatom biomass (Eq. (2)). The total grazing rate on diatoms by zooplankton exceeds the diatom total growth rate below the depth of 47.5, 32.5, 27.5, 32.5, 32.5, 47.5 and 62.5 m in Cases 1-1, 1-2, 1-3, 1-4, 1-5, 1-6 and 1-7, respectively (Table 2). The depth is similar to the modeled compensation depth by 5 m in any case. The higher total grazing rate on diatoms by zooplankton than the diatom total growth rate means no accumulation or decrease of

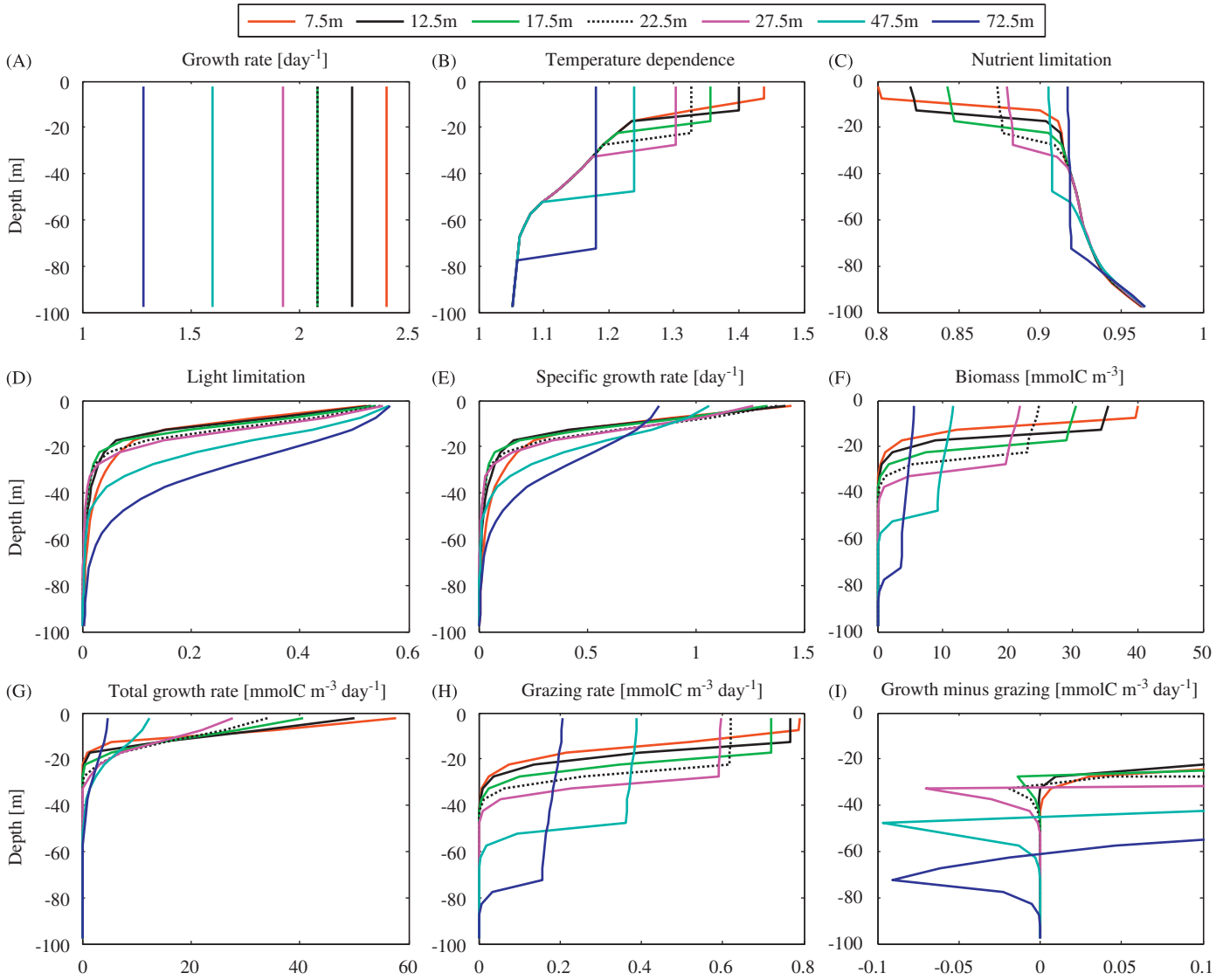

Fig. 6. Vertical profile of (A) Term 1 (the maximum diatom growth rate V_{maxL}) (day^{-1}), (B) Term 2 (temperature dependence exp($k_L T$)), (C) Term 3 (nutrient limitation), (D) Term 4 (light limitation), (E) diatom-specific growth rate (the product of Terms 1–4) (day^{-1}), (F) Term 5 (diatom biomass) (mmol C m^{-3}), (G) diatom total growth rate (the product of Terms 1–5) (mmol C m^{-3} day^{-1}), (H) total grazing rate on diatoms by zooplankton (ZL and ZP) (mmol C m^{-3} day^{-1}) and (I) diatom total growth rate minus total grazing rate on diatoms by zooplankton ((G) and (H)), on the date when the maximum surface chlorophyll appears (on Days 11, 12, 13, 13, 14, 16 and 18 in Cases 1-1, 1-2, 1-3, 1-4, 1-5, 1-6 and 1-7, respectively); all in Experiment 1 varying MLD. For the actual Terms 1–5 see Eq. (1) in the main text.

Table 2
Modeled (1) MLD, (2) compensation depth (CD), and (3) depth at which diatom grazing rate exceeds diatom total growth rate, in Experiment 1 (for variation of MLD).

	Case 1-1	Case 1-2	Case 1-3	Case 1-4	Case 1-5	Case 1-6	Case 1-7
(1) MLD (m)	7.5	12.5	17.5	22.5	27.5	47.5	72.5
(2) Compensation depth (CD) (m)	42.5	27.5	22.5	27.5	27.5	42.5	62.5
(3) Depth at which diatom grazing rate exceeds diatom total growth rate (m)	47.5	32.5	27.5	32.5	32.5	47.5	62.5

The compensation depth is defined as the depth at which PAR is equal to 1% of the surface PAR.

diatom biomass at the depth, showing that the diatom growth is regulated by both light limitation and grazing pressure below the compensation depth even during the iron-induced diatom bloom prime, which is irrespective of the MLD.

3.2. Biogeochemical responses to initial plankton conditions

With different initial diatom biomasses (Experiment 2), the iron-induced diatom bloom occurs earlier and is larger with higher initial diatom concentration (Fig. 7-1(C)). The decrease of $Si(OH)_4$ (Fig. 3(B)) is the weakest with the lowest initial diatom biomass (Case 2-1; 0.001 times the standard initial diatom biomass). With different initial mesozooplankton biomasses (Experiment 3), the iron-induced diatom bloom occurs earlier and is larger with lower initial mesozooplankton biomass (Fig. 7-2(C)). The surface chlorophyll increases by a factor of 75 with lower initial mesozooplankton biomass (Cases 3-1 and 3-2; 0.01 and 0.1 times the standard initial mesozooplankton biomass; Fig. 3(C)), but its increase is only by a factor of 30 with the highest

initial mesozooplankton biomass (Case 3-7; 30 times the standard initial mesozooplankton biomass; Fig. 3(C)). The decrease of $Si(OH)_4$ (Fig. 3(C)) is the weakest with the highest initial mesozooplankton biomass (Case 3-7).

The iron-induced diatom bloom is triggered by a rapid increase in the diatom-specific growth rate (equivalent to diatom total growth rate divided by diatom biomass; Eq. (1) and Figs. 7-1(A) and -2(A)). The diatom-specific growth rate increases from 0.6 (day^{-1}) on Day 0 to up to 1.9 (day^{-1}) on about Day 5 in all cases, which reflects the effects of iron enrichment on diatom growth. The diatom-specific growth rate returns to the initial level of 0.6 (day^{-1}) after termination of iron enrichment. This result indicates that iron concentration controls diatom-specific growth rates regardless of initial plankton biomass.

Compared with the diatom-specific growth rate, specific grazing rate on diatoms by mesozooplankton (total grazing rate on diatoms by mesozooplankton divided by mesozooplankton biomass; Eq. (2)) is different among the cases (Figs. 7-1(B) and -2(B)). The specific grazing rate increases rapidly from very low values to close to 0.8 (day^{-1}) in all cases. The lower specific grazing rate at the first phase of simulation (from Day 0 to 10) in Cases 2-1 and 2-2 (Fig. 7-1(B)) is initially due to lower diatom concentration. The slow accumulation of diatom biomass (Cases 2-1 and 2-2; Fig. 7-1(C)) results in a delayed peak of the specific grazing rate, which is determined by diatom concentration. On the other hand, higher initial mesozooplankton biomass (Cases 3-6 and 3-7) results in lower diatom biomass (Fig. 7-2(C)) and a lower specific grazing rate of mesozooplankton (Fig. 7-2(B)) during the first phase of iron infusion, which is initially due to higher grazing pressure on diatoms. With lower initial mesozooplankton biomass (Cases 3-1 and 3-2), by contrast, diatoms at the first phase can escape from high grazing pressure and produce a stronger bloom (Fig. 7-2(C)). The high biomass of diatoms provides an adequate food supply for mesozooplankton, which results in an earlier peak of the specific grazing rate and a gradual increase in mesozooplankton biomass (Figs. 7-2(B) and (D)).

The time series of diatom total growth rate is similar to that of the diatom concentration in both Experiments 2 and 3 (Figs. 7-1(C), (E) and -2(C), (E)). The maximum diatom total growth rate appears earlier and higher with higher initial diatom concentration (Fig. 7-1(E)). For the different cases with initial mesozooplankton biomass, the diatom total growth rate is higher and reaches its maximum earlier with lower initial mesozooplankton biomass (Cases 3-1 and 3-2; Fig. 7-2(E)).

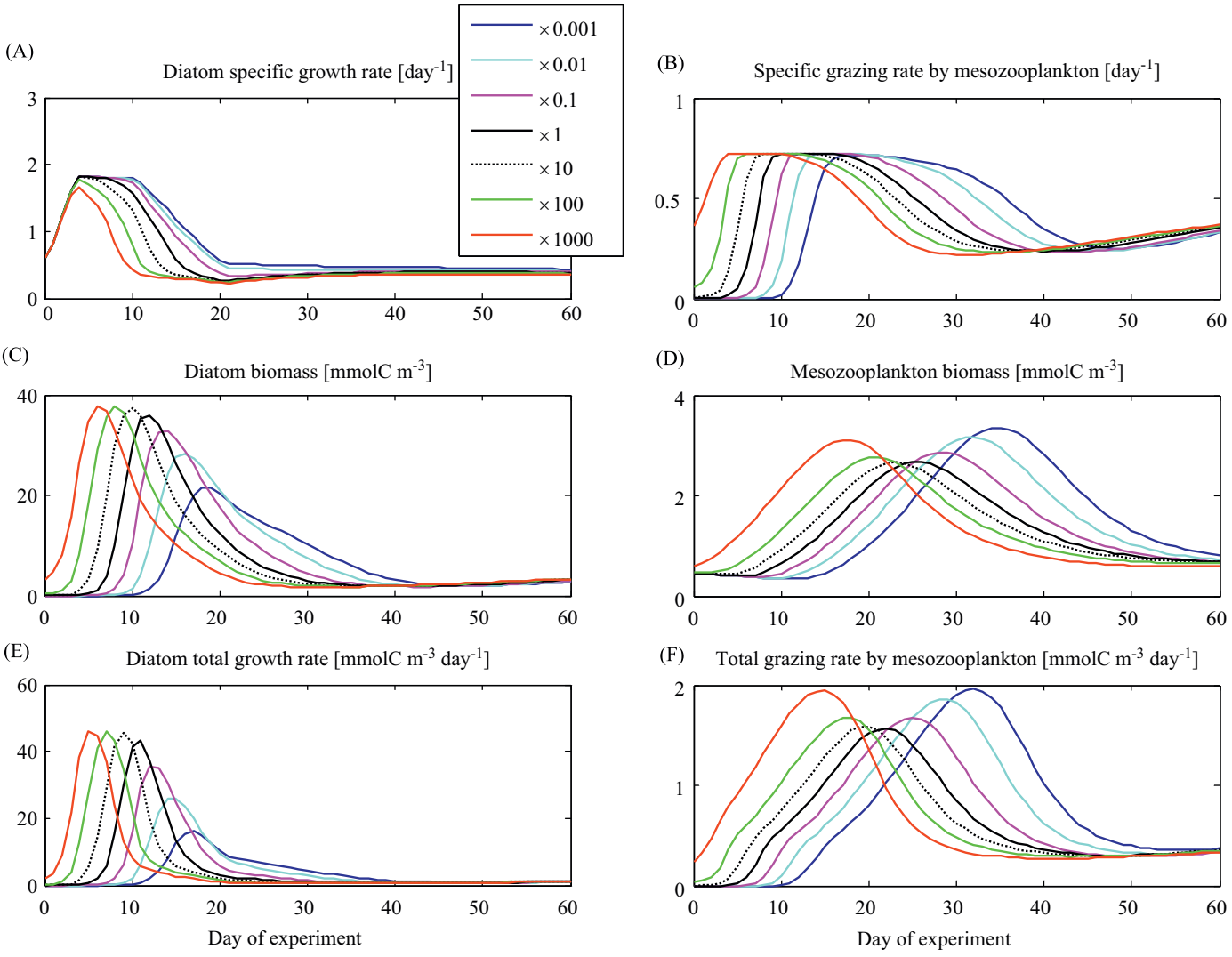

Fig. 7. (1) Time series of modeled surface (A) diatom-specific growth rate (day^{-1}), (B) specific grazing rate on diatoms by mesozooplankton (day^{-1}), (C) diatom biomass (mmol C m^{-3}), (D) mesozooplankton biomass (mmol C m^{-3}), (E) diatom total growth rate (mmol C m^{-3} day^{-1}) and (F) total grazing rate on diatoms by mesozooplankton (mmol C m^{-3} day^{-1}) all in Experiment 2 varying the initial diatom biomass PL. (2) Same as (1) but for Experiment 3 varying the initial mesozooplankton biomass ZL.

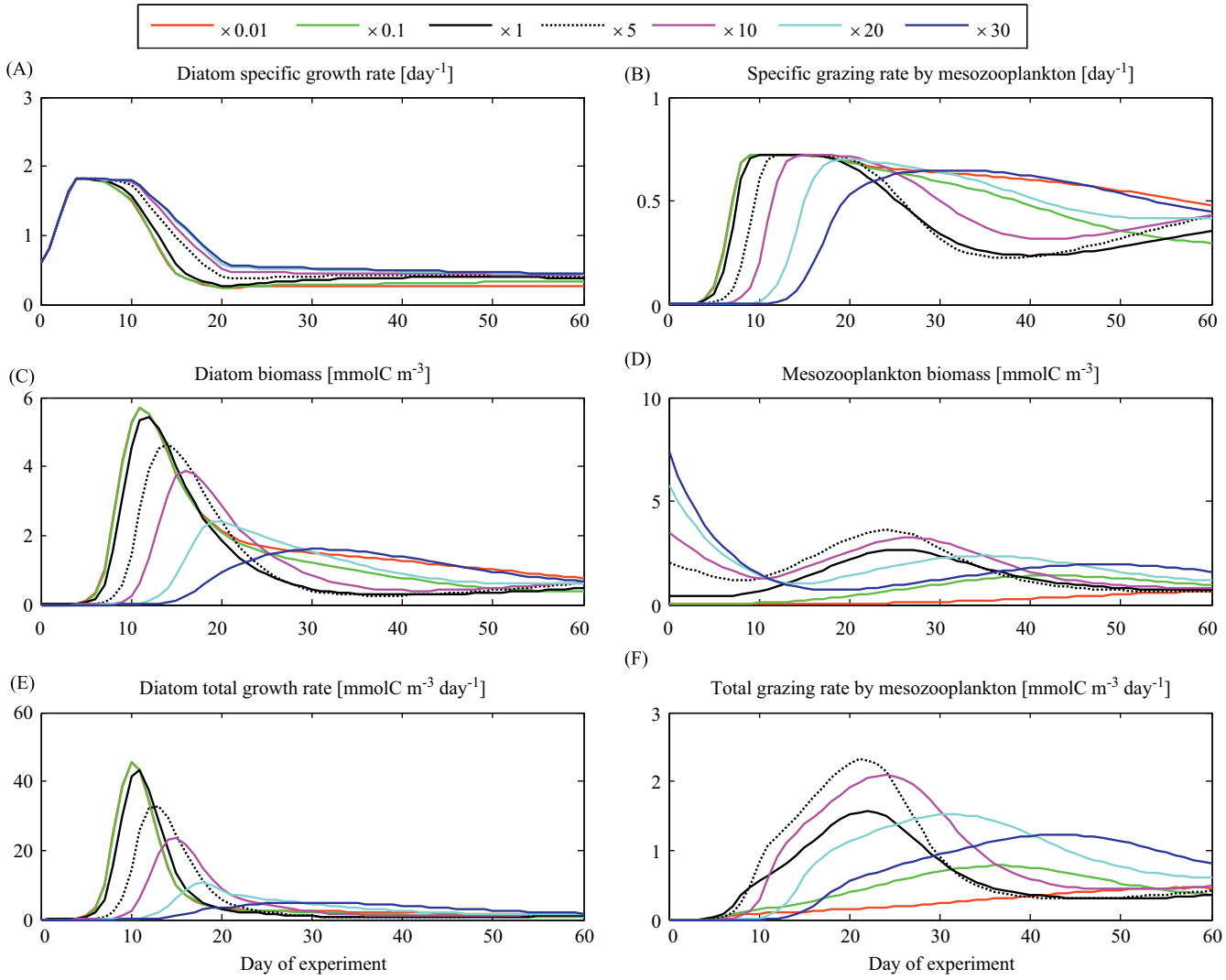

Fig. 7. (*Continued*)

In Experiment 2, the maximum total grazing rate on diatoms by mesozooplankton (0.24–0.30 (day^{-1})) is similar among the cases, but the timing of the peak is earlier with higher initial diatom concentrations (Fig. 7-1(F)). The delayed peak of grazing on diatoms with lower initial diatom biomass (Cases 2-1 and 2-2) is due to slower accumulation of diatom biomass (Figs. 7-1(C) and (F)). In Experiment 3, however, the total grazing rate varies substantially not only in timing but also in magnitude (Fig. 7-2(F)). With the highest initial mesozooplankton biomass (Case 3-7), the total grazing rate on diatoms is low and peaks on Day 45. This is because of the slower buildup of diatom biomass (Fig. 7-2(C)). It seems that two cases with intermediate initial mesozooplankton biomass (Cases 3-4 and 3-5) produce the highest total grazing rate on diatoms, which results from high diatom and mesozooplankton biomass (Figs. 7-2(C), (D) and (F)). The intermediate initial mesozooplankton biomass could yield relatively high biomass for both diatoms and mesozooplankton, suggesting strong trophic links at any intermediate grazer density. This finding is in good agreement with fundamental theory in revealing that on food-web dynamics away from equilibrium, weak to intermediate strength links are important in promoting community persistence and stability because weak links act to dampen oscillations between consumers and resources (e.g., McCann et al., 1998; Van der Meer, 2004). Therefore, the initial level of mesozooplankton biomass, i.e., the condition of higher tropic levels at the time of iron infusion, plays an important role in determining the intensity of the iron-induced diatom bloom (Tsuda et al., 2007) and total increase of mesozooplankton. This is consistent with results from recent iron-fertilization experiments in the Southern Ocean (the Antarctic Circumpolar Current (EisenEx; Schultes et al., 2006) and the European iron-fertilization experiment (EIFEX; Jansen et al., 2006), which revealed that high feeding activity of diatom's grazers prior to and during the iron-induced diatom bloom plays a large role in shaping diatom population dynamics. The top-down (grazing) control on the iron-induced diatom bloom is evident even in the Southern Ocean in which the response has been considered to be relatively lower because of the substantially lower water temperature.

3.3. *Relative impacts of physical and biological conditions*

The maximum surface chlorophyll, ΔNO_3, $\Delta Si(OH)_4$, ΔDIC, $\Delta pCO_{2\,sea}$, ΔNCP and ΔEP are compared among Experiments 1–3

Table 3
Difference in each variable with Experiments 1–6.

	Experiment 1 (MLD)	Experiment 2 (PL)	Experiment 3 (ZL)	Experiment 4 (PS)	Experiment 5 (ZS)	Experiment 6 (ZP)
Surface maximum chlorophyll ($mg\,Chl\,m^{-3}$)	20 (10)	14 (3)	15 (4)	6 (2)	1 (1)	2 (1)
Surface maximum NO_3 decrease ($mmol\,N\,m^{-3}$)	14 (13)	8 (2)	11 (4)	10 (3)	3 (1)	2 (1)
Surface maximum $Si(OH)_4$ decrease ($mmol\,Si\,m^{-3}$)	26 (7)	10 (2)	14 (2)	7 (1)	2 (1)	2 (1)
Surface maximum DIC decrease ($mmol\,C\,m^{-3}$)	56 (11)	37 (3)	54 (10)	31 (2)	13 (1)	11 (1)
Maximum $pCO_{2\,sea}$ decrease (μatm)	109 (8)	67 (2)	105 (7)	55 (2)	30 (1)	22 (1)
Column-integrated chlorophyll ($mg\,Chl\,m^{-2}$)	38 (2)	8 (1)	53 (3)	5 (1)	49 (4)	7 (1)
Maximum net community production ($mg\,C\,m^{-2}\,day^{-1}$)	3100 (4)	2509 (3)	3789 (11)	2506 (2)	1434 (2)	905 (1)
Maximum export production ($mg\,C\,m^{-2}\,day^{-1}$)	1651 (7)	1438 (3)	1951 (15)	1126 (2)	532 (1)	421 (1)

Differences are obtained by subtracting a minimum value from a maximum value. The ratio of maximum value divided by minimum value is shown in parentheses. Experiments were for variations of MLD (Experiment 1), initial diatom biomass PL (Experiment 2), initial mesozooplankton biomass ZL (Experiment 3), initial non-diatom small phytoplankton biomass PS (Experiment 4), initial microzooplankton biomass ZS (Experiment 5) and initial predatory macrozooplankton biomass ZP (Experiment 6).

(Table 3; Figs. 5-1 and -2). It is interesting that the magnitude of the diatom bloom in terms of the surface maximum chlorophyll (Fig. 5-2(A)) differs only by a factor of 2.9 in Experiment 2, although the initial diatom biomass differs by an order of 10^6. For most of the variables, the fluctuation is the greatest in Experiment 1 (Table 3). For the column-integrated chlorophyll, ΔNCP and ΔEP, however, the fluctuation range is much larger in Experiment 3 than in Experiment 1. Therefore, this modeling study suggests that MLD is generally the most predominant factor, but the initial mesozooplankton biomass is also very crucial, especially in controlling the column-integrated variables such as biomass, NCP and EP. In assessing the efficiency of iron-fertilization experiments, the amount of atmospheric CO_2 that is absorbed by oceans can be a good proxy, and therefore, we should pay more attention to the EP in the deep water and the ratio of the EP to the NCP (e-ratio).

We have also examined the effects of iron enrichments on the phytoplankton community in response to different initial non-diatom small phytoplankton (Experiment 4), microzooplankton (Experiment 5) and predatory macrozooplankton (Experiment 6) conditions, by changing from 0.001 to 1000 times (Experiment 4) and from 0.01 to 30 times (Experiments 5 and 6) the standard initial condition used in Fujii et al. (2005), respectively (Tables 1 and 3). The profile of each variable vs. initial phytoplankton biomass in Experiment 4 is a mirror image of that in Experiment 2 (Fig. 5-2), showing that the increase in the initial diatom biomass corresponds to the decrease in the initial non-diatom small phytoplankton biomass. The fluctuation is mostly smaller in Experiment 4 than in Experiment 2 except for ΔNO_3 (Table 3), indicating that the modeled ΔNO_3 is more sensitive to the initial non-diatom small phytoplankton than to the initial diatom biomass. The overall model results (Table 3) show that the plankton ecosystem is not very sensitive to variations in initial non-diatom small phytoplankton (Experiment 4), initial microzooplankton (Experiment 5) or initial predatory macrozooplankton (Experiment 6). Therefore the findings of the latter Experiments 4–6 will not further be discussed or shown in graphics.

4. Concluding remarks

Using a marine ecosystem model, we examined the influence of initial plankton conditions and MLD on the biogeochemistry of HNLC regions. The modeled responses to the same iron enhancement treatment differed dramatically according to different MLDs. The observed inverse relationship between the maximum surface chlorophyll and MLD of eight different *in situ* experiments is well simulated by variation of MLD for just one such experiment, even though other conditions such as sea-surface irradiance are set similarly among the simulations, and even though the model is applied to merely one *in situ* iron-enrichment experiment (SEEDS). This shows that the MLD is the predominant factor in controlling iron-induced biogeochemical responses, as mentioned by de Baar et al. (2005).

The significant difference in the maximum surface chlorophyll with MLD is primarily caused by diatom concentration in the mixed layer, which is determined by vertical mixing. Other factors that result from the change of MLD, such as temperature, light and nutrients, play lesser roles on the formation of surface chlorophyll maximum. The iron-induced diatom bloom is severely restricted below the compensation depth due to both light limitation and grazing pressure, irrespective of the MLD.

The initial biomass of mesozooplankton is also important in determining the iron-induced biogeochemical responses. Higher initial mesozooplankton biomass yields high grazing pressure on diatoms, which results in less accumulation of diatom biomass during the iron-enrichment period. Although the influences are less significant than those of the MLD in most variables, the column-integrated chlorophyll, NCP and EP are more strongly determined by the initial mesozooplankton biomass. As EP is a key variable for assessing the efficiency of oceanic carbon uptake by iron experiments, the importance of grazing to the outcome of iron experiments should be more worthy of attention. Also we need to keep in mind that efficiency could be evaluated using different variables, i.e., with surface values vs. column-integrated values, as is also suggested in this study that unlike the maximum chlorophyll, the highest column-integrated chlorophyll appears with intermediate MLD cases.

The initial biomass of diatoms is also important but is not as crucial as the MLD and the initial mesozooplankton biomass in determining the overall plankton community response to iron enrichments. Diatom blooms occur in any initial diatom concentrations due to the very fast diatom growth rates stimulated by iron addition. But the iron-induced diatom growth may not result in the accumulation of diatom biomass under the high grazing pressure imposed by extremely high initial mesozooplankton biomass.

This modeling study suggests that in addition to the MLD, initial plankton biomass, especially principal grazers on diatoms, is a crucial factor in the response of phytoplankton community to iron enrichments. The modeling result may account for the different biological responses of SEEDS vs. SEEDS II, which were conducted in the same location and in the same season of the year. The notably higher surface chlorophyll during SEEDS than during SEEDS II may primarily be due to the significantly

(3–5 times) lower initial mesozooplankton biomass at the beginning of SEEDS compared with SEEDS II, because other factors such as the initial diatom biomass and the physical and chemical environmental conditions were very similar (Tsuda et al, 2007). The result from this study is also consistent with the hypothesis that phytoplankton bloom development in the Southern Ocean is highly sensitive to both physical and biological parameters that determine vertical mixing and phytoplankton loss rates mainly due to grazing pressure (Mitchell et al., 1991; Sakshaug et al., 1991; Lancelot et al., 1993). This suggests that the modeling results from this study could be applied to other HNLC regions and factors affecting the potential outcome of iron-fertilization in these regions. The initial state of the plankton community, along with physical and chemical environmental conditions, should be taken into account when designing future iron-enrichment experiments and observational plans.

Acknowledgements

We thank Drs. Hein de Baar, Pedro Branco, Atsushi Tsuda, Hiroaki Saito, Naoki Yoshie, Yasuhiro Yamanaka, James McCleave and Anthony Chittenden, and two reviewers for providing helpful and constructive comments. This research was supported by a National Science Foundation grant (OCE-0137272) to F. Chai. M. Fujii was supported by MEXT through Special Coordination Funds for Promoting Sciences and Technology. This paper resulted from the international collaborative field project developed under the umbrella of PICES, through its Advisory Panel on the Iron Fertilization Experiment in the Subarctic Pacific Ocean (IFEP).

References

Assmy, P., Henjes, J., Klaas, C., Smetacek, V., 2007. Mechanisms determining species dominance in a phytoplankton bloom induced by the iron fertilization experiment EisenEx in the Southern Ocean. Deep-Sea Research I 54, 340–362.

Bakker, D.C.E., Bozec, Y., Nightingale, P.D., et al., 2005. Iron and mixing affect biological carbon uptake in SOIREE and EisenEx, two Southern Ocean iron fertilization experiments. Deep-Sea Research I 52, 1001–1019.

Banse, K., 1990. Does iron really limit phytoplankton production in the offshore subarctic Pacific?. Limnology and Oceanography 35, 772–775.

Boyd, P.W., Watson, A.J., Law, C.S., et al., 2000. A mesoscale phytoplankton bloom in the polar Southern Ocean stimulated by iron fertilization. Nature 407, 695–702.

Boyd, P.W., Law, C.S., Wong, C.S., et al., 2004. The decline and fate of an iron-induced subarctic phytoplankton bloom. Nature 428, 549–553.

Boyd, P.W., Jickells, T., Law, C.S., et al., 2007. Mesoscale iron-enrichment experiments 1993–2005: synthesis and future directions. Science 315, 612–617.

Chai, F., Dugdale, R.C., Peng, T.-H., Wilkerson, F.P., Barber, R.T., 2002. One-dimensional ecosystem model of the equatorial Pacific upwelling system. Part I: model development and silicon and nitrogen cycle. Deep-Sea Research II 49, 2713–2745.

Chai, F., Jiang, M.-S., Chao, Y., Dugdale, R.C., Chavez, F., Barber, R.T., 2007. Modeling responses of diatom productivity and biogenic silica export to iron enrichment in the equatorial Pacific Ocean. Global Biogeochemical Cycles 21, GB3S90, doi:10.1029/2006GB002804.

Coale, K.H., Johnson, K.S., Fitzwater, S.E., et al., 1996. A massive phytoplankton bloom induced by an ecosystem-scale iron fertilization experiment in the equatorial Pacific Ocean. Nature 383, 495–501.

Coale, K.H., Johnson, K.S., Chavez, F.P., et al., 2004. Southern Ocean iron enrichment experiment: carbon cycling in high- and low-Si waters. Science 304, 408–414.

de Baar, H.J.W., Boyd, P.W., Coale, K.H., et al., 2005. Synthesis of iron fertilization experiments: from the iron age in the age of enlightenment. Journal of Geophysical Research 110, C09S16, doi:10.1029/2004JC002601.

Denman, K.L., Peña, M.A., 1999. A coupled 1-D biological/physical model of the northeast subarctic Pacific Ocean with iron limitation. Deep-Sea Research II 46, 2877–2908.

Fujii, M., Nojiri, Y., Yamanaka, Y., Kishi, M.J., 2002. A one-dimensional ecosystem model applied to time series station KNOT. Deep-Sea Research II 49, 5441–5461.

Fujii, M., Yoshie, N., Yamanaka, Y., Chai, F., 2005. Simulated biogeochemical responses to iron enrichments in three high nutrient, low chlorophyll (HNLC) regions. Progress in Oceanography 64, 307–324, doi:10.1016/j.pocean.2005.02.017.

Gervais, F., Riebesell, U., Gorbunov, M.Y., 2002. Changes in primary productivity and chlorophyll a in response to iron fertilization in the southern Polar Frontal Zone. Limnology and Oceanography 47, 1324–1335.

Hall, J.A., Safi, K., 2001. The impact of in situ Fe fertilization on the microbial food web in the Southern Ocean. Deep-Sea Research II 48, 2591–2613.

Hannon, E., Boyd, P.W., Silvoso, M., Lancelot, C., 2001. Modeling the bloom evolution and carbon flows during SOIREE: implications for future in situ iron-enrichments in the Southern Ocean. Deep-Sea Research II 48, 2745–2773.

Jansen, S., Klaas, C., Kragefsky, S., Von Harbou, L., Bathmann, U., 2006. Reproductive response of the copepod *Rhincalanus gigas* to an iron-induced phytoplankton bloom in the Southern Ocean. Polar Biology 29, 1039–1044.

Lancelot, C., Mathot, S., Veth, C., de Baar, H.J.W., 1993. Factors controlling phytoplankton ice-edge blooms in the marginal ice-zone of the northwestern Weddell Sea during sea ice retreat 1988: field observations and mathematical modeling. Polar Biology 13, 377–387.

Landry, M.R., Constantinou, J., Latasa, M., Brown, S.L., Bidigare, R.R., Ondrusek, M.E., 2000a. Biological response to iron fertilization in the eastern equatorial Pacific (IronEx II). III. Dynamics of phytoplankton growth and microzooplankton grazing. Marine Ecology Progress Series 201, 57–72.

Landry, M.R., Ondrusek, M.E., Tanner, S.J., Brown, S.L., Constantinou, J., Bidigare, R.R., Coale, K.H., Fitzwater, S., 2000b. Biological response to iron fertilization in the eastern equatorial Pacific (IronEx II). I. Microplankton community abundances and biomass. Marine Ecology Progress Series 201, 27–42.

Laws, E.A., Falkowski, P.G., Smith Jr., W.O., Ducklow, H., McCarthy, J.J., 2000. Temperature effects on export production in the open ocean. Global Biogeochemical Cycles 14, 1231–1246.

Martin, J.H., 1990. Glacial–interglacial CO_2 change: the iron hypothesis. Paleoceanography 5, 1–13.

Martin, J.H., Fitzwater, S.E., 1988. Iron deficiency limits phytoplankton growth in the north-east Pacific subarctic. Nature 331, 341–343.

McCann, K., Hastings, A., Huxel, G.R., 1998. Weak trophic interactions and the balance of nature. Nature 395, 794–798.

Mitchell, B.G., Brody, E.A., Holm-Hansen, O., McClain, C., Bishop, J., 1991. Light limitation of phytoplankton biomass and macronutrient utilization in the Southern Ocean. Limnology and Oceanography 36, 1662–1677.

Redfield, A.C., Ketchum, B.A., Richards, F.A., 1963. The influence of organisms on the composition of seawater. In: Hill, M.H. (Ed.), The Sea. Wiley, New York, pp. 26–77.

Rollwagen Bollens, G.C., Landry, M.R., 2000. Biological response to iron fertilization in the eastern equatorial Pacific (IronEx II). II. Mesozooplankton abundance, biomass, depth distribution and grazing. Marine Ecology Progress Series 201, 43–56.

Saito, H., Ota, T., Suzuki, K., Nishioka, J., Tsuda, A., 2006. Role of heterotrophic dinoflagellate *Gyrodinium* sp. in the fate of an iron induced diatom bloom. Geophysical Research Letter 33, L09602, doi:10.1029/2005GL025366.

Saito, H., Suzuki, K., Hinuma, A., et al., 2005. Responses of microzooplankton to in situ iron fertilization in the western subarctic Pacifcic (SEEDS). Progress in Oceanography 64, 223–236, doi:10.1016/j.pocean.2005.02.010.

Saito, H., Tsuda, A., Nojiri, Y., Aramaki, T., Ogawa, H., Yoshimura, T., Imai, K., Kudo, I., Nishioka, J., Ono, T., Suzuki, K., Takeda, S., 2009. Biogeochemical cycling of N and Si during the mesoscale iron-enrichment experiment in the western subarctic Pacific (SEEDS-II). Deep-Sea Research II 56 (26), 2852–2862.

Sakshaug, E., Slagstad, D., Holm-Hansen, O., 1991. Factors controlling the development of phytoplankton blooms in the Antarctic Ocean—a mathematical model. Marine Chemistry 35, 259–271.

Schultes, S., Verity, P.G., Bathmann, U., 2006. Copepod grazing during an iron-induced diatom bloom in the Antarctic Circumpolar Current (EisenEx); I. Feeding patterns and grazing impact on prey populations. Journal of Experimental Marine Biology and Ecology 338, 16–34.

Suzuki, K., Hinuma, A., Saito, H., Kiyosawa, H., Liu, H., Saino, T., Tsuda, A., 2005. Responses of phytoplankton and heterotropic bacteria in the northwest subarctic Pacific to in situ iron fertilization as estimated by HPLC pigment analysis and flow cytometry. Progress in Oceanography 64, doi:10.1016/j.pocean.2005.02.007.

Takeda, S., Tsuda, A., 2005. An in situ iron-enrichment experiment in the western subarctic Pacific (SEEDS): introduction and summary. Progress in Oceanography 64, 95–109, doi:10.1016/j. pocean.2005.02.004.

Tsuda, A., Takeda, S., Saito, H., et al., 2007. Evidence for the grazing hypothesis: grazing reduces phytoplankton responses of the HNLC ecosystem to iron enrichment in the western subarctic Pacific (SEEDS II). Journal of Oceanography 63, 983–984.

Tsuda, A., Takeda, S., Saito, H., et al., 2003. A mesoscale iron enrichment in the western subarctic Pacific induces a large centric diatom bloom. Science 300, 958–961.

Van der Meer, J., 2004. Coupled oscillations in food webs: balancing competition and mutualism in simple ecological models. The American Naturalist 163, 857–867.

Yamanaka, Y., Yoshie, N., Fujii, M., Aita, M.N., Kishi, M.J., 2004. An ecosystem model coupled with nitrogen–silicon–carbon cycles applied to Station A7 in the Northwestern Pacific. Journal of Oceanography 60, 227–241.

Yoshie, N., Fujii, M., Yamanaka, Y., 2005. Ecosystem changes with the iron fertilization in the western North Pacific simulated by a one-dimensional ecosystem model. Progress in Oceanography 64, 283–306, doi:10.1016/j.pocean.2005.02.014.